ChemElectroChem

Research Article
doi.org/10.1002/celc.202300121

Chemistry Europe
European Chemical Societies Publishing

www.chemelectrochem.org

Impact of the Carbon Substrate for Gas Diffusion Electrodes on the Electroreduction of CO_2 to Formate

Verena Theußl,*[a, b] Henning Weinrich,[a] Christine Heume,[a, b] Krzysztof Dzieciol,[a] Bernhard Schmid,[a] Hans Kungl,[a] Hermann Tempel,[a] and Rüdiger-A. Eichel[a, b]

Aiming to advance the technical maturity of CO_2 electrolysis to formic acid, various gas diffusion layers (GDLs) are investigated for their suitability as carbon-based substrate for gas diffusion electrodes (GDEs) and their effect on the electroreduction of CO_2 to formate. Particular attention lies on the elucidation for the effect of the GDL thickness, hydrophobic treatment, and presence of a microporous layer (MPL) on the GDE performance in terms of Faradaic efficiency. Based on the investigation it is found that the GDL thickness has no discernible influence on the Faradaic efficiency, while a GDE with a hydrophobic treatment of 10% PTFE outperforms a GDE based on a GDL with 30% PTFE. Furthermore, the presence of a MPL is found to be of marked importance to achieve relevant current densities given its effect on the focus of the catalyst layer on the GDE surface after spray coating, the wetting, and the electrical conductivity.

Introduction

Among the various techniques to reduce CO_2 emissions in a vital attempt to mitigate global warming,[1–3] Power-to-X is a promising approach for CO_2 valorization.[4–7] Here, the X is a carbonaceous compound derived from anthropogenic CO_2, water and renewably generated electricity. Based on Power-to-X, a variety of different chemicals such as CO,[8–10] syngas[11] and formic acid[12–15] is available on a renewable basis, potentially allowing for the implementation of sustainable CO_2-to-X value chains in the near future. To pave the way to this desirable future, a multitude of challenges must be overcome. These challenges lie in the stability of components and the boundary conditions of the underlying processes.[16,17] Focusing on formic acid as a base chemical with high economic value in food and textile industry,[18] Power-to-X has the chance to become economically competitive as compared to conventional routes. However, its implementation still requires higher energy efficiency, current density, product selectivity and longevity of the electrolyzers compared to the state-of-the-art.[16,17] Meeting these goals requires improvements to various components of the cell, with the cathode currently bearing the largest development potential.

The most frequent approach for the implementation of CO_2 electroreduction consists in the application of carbon paper-based gas diffusion electrodes (GDEs)[19–21] as a cathode in a membrane reactor flow cell.[22,23] Like GDEs for fuel cells,[24,25] the cathodes for CO_2-to-formate or formic acid typically use a design where a catalyst layer is deposited on top of a carbon fiber substrate. The carbon fiber substrate is used as a gas diffusion layer (GDL) and may or may not include a microporous layer (MPL, Figure 1).[21,26] The performance of the corresponding GDE is highly dependent on the electrode architecture and material properties, including the choice of the GDL. Typical properties of the GDL are (i) the presence of an MPL, (ii) the thickness and (iii) the hydrophobic treatment for both the carbon fiber substrate and the possible MPL. Furthermore, in a GDE the effects of the GDL are superimposed with the properties of the catalyst layer as well as its thickness, the deposition method, and the applied materials. Accordingly, in the literature a multitude of papers report on the design and investigation of GDEs for Power-to-X in general and CO_2-to-formate in particular.[27–31] However, there is no dedicated study for the impact of the GDL on the performance of GDEs for CO_2-to-formate, despite the unique requirement of the GDE

[a] V. Theußl, Dr. H. Weinrich, C. Heume, Dr. K. Dzieciol, B. Schmid, Dr. H. Kungl, Dr. H. Tempel, Prof. Dr. R.-A. Eichel
Institute of Energy and Climate Research – Fundamental Electrochemistry (IEK-9)Forschungszentrum Jülich GmbH
Wilhelm-Johnen Straße, 52428 Jülich (Germany)
E-mail: v.theussl@fz-juelich.de
[b] V. Theußl, C. Heume, Prof. Dr. R.-A. Eichel
Institute of Physical Chemistry
RWTH Aachen University
Landoltweg 2, 52074 Aachen (Germany)

Supporting information for this article is available on the WWW under https://doi.org/10.1002/celc.202300121

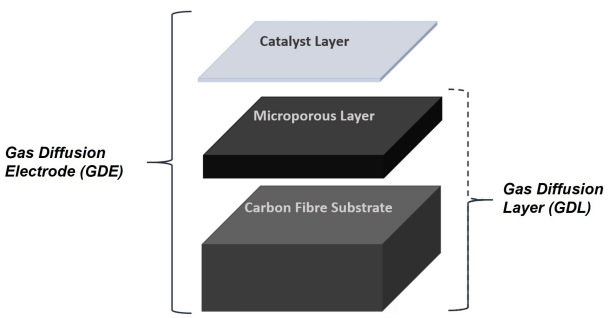

Figure 1. Schematic representation of the investigated gas diffusion electrodes (GDEs) based on a commercial gas diffusion layer (GDL) by Toray Industries, Japan.

operating in formate solutions. In a recent study for the pronounced effect of the product composition on the reaction conditions, the electrode wetting has been reported to differ vastly for diluted formic acid as compared to other products of CO_2 electrolysis such as methanol, ethanol and propanol. The difference is explained by the higher surface tension of formic acid as compared the alcohols.[32] Furthermore, due to the ionic character of formate as compared to gaseous[33] products of electrolysis such as CO, the optimum architecture of GDEs for CO_2-to-formate might differ from GDEs for CO_2-to-CO. This might be caused by different release modes, i.e., migration enhanced diffusion towards the anode for formate vs. diffusion in the catholyte and emission into the gas phase for CO. Accordingly, for formate, major differences for the impact of the GDL on the GDE performance as compared to previous studies for gaseous target molecules such as CO[34–37] can be expected.

In this study, the impact of the GDL on the performance of spray-coated GDEs for the electrochemical reduction of CO_2 to formate was investigated. For the investigation, commercial SnO_2 nanoparticles were applied as a CO_2 electroreduction catalyst.[38] Furthermore, a commercial, gas-fed electrolyzer setup with static electrolyte was used, which allows for a rapid and highly reproducible screening of custom-made GDEs due to the simple, but precise assembly of the cell.[39] The screening focuses on Toray Paper GDLs exclusively, given their vast coverage in literature, broad variety and good availability worldwide. Furthermore, pretests in comparison with other commercial GDLs such as SIGRACET have shown the suitability of Toray Paper for the intended study in the unsupported gas compartment of the test setup. Table 1 provides an overview of the investigated GDLs, which differ in the following three properties: the GDL thickness, the hydrophobic treatment, and the presence of an MPL. These three properties may have influence on the electrical conductivity, the wetting, and the CO_2 supply for the catalyst. All of this is to be investigated by short-term cathode testing to readily elucidate the effect of the GDL on the performance of GDEs for CO_2-to-formate.

Table 1. Overview and *abbreviations* of the investigated gas diffusion layers (GDLs, designation according to manufacturer, TGP-H-xxx, Toray Industries, Japan) either with (w) or without (w/o) microporous layer (MPL) and either using 10% or 30% PTFE as a hydrophobic treatment of the carbon fiber substrate. ([1] Specification according to manufacturer).

GDL		Thickness[1]	
		190 µm (+60 µm MPL)	370 µm (+60 µm MPL)
w/o MPL	10% PTFE	TGP-H-060 (10% PTFE) *TP-060 (10%)*	TGP-H-120 (10% PTFE) *TP-120 (10%)*
	30% PTFE	TGP-H-060 (30% PTFE) *TP-060 (30%)*	TGP-H-120 (30% PTFE) *TP-120 (30%)*
w MPL	30% PTFE	TGP-H-060 MPL (30% PTFE) *TP-060 MPL (30%)*	TGP-H-120 MPL (30% PTFE) *TP-120 MPL (30%)*

Results and Discussion

Physico-chemical characterization

Figure 2 and Figures S1-2 depict SEM images of the pristine GDLs as well as the GDEs before and after the electrochemical testing. Figure 2 shows exemplary SEM-images for TP-060 (30%) and TP-060 MPL (30%). In Figure 2a and d, the SEM images of the pristine GDLs show the typical appearance of the carbon fiber substrate and the MPL before catalyst deposition. In Figure 2d the MPL shows cracks in the pristine state of the GDL already.[40,41] Figure 2b and e provide an overview for the catalyst coated GDLs, i.e., the GDEs before the electrochemical testing. In case of TP-060 (30%, Figure 2b), the catalyst

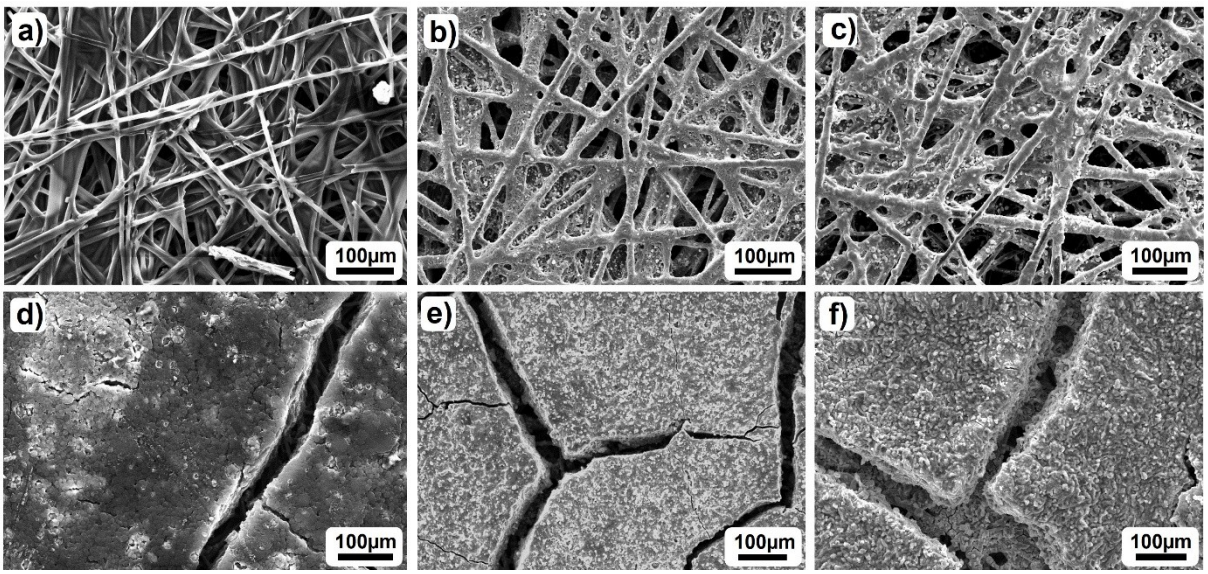

Figure 2. Exemplary SEM images of the pristine gas diffusion layers (GDLs) and the gas diffusion electrodes (GDEs) before and after use. a–c) Images for TP-060 (30%), d–f) Images for TP-060 MPL (30%). A), d) Pristine GDLs (without catalyst). B), e) GDEs before electrochemical testing. C), f) GDEs after electrochemical testing. (Additional images for other samples as well as EDX maps can be found in Figures S1–3).

deposition leads to a thick decoration of the carbon fibers, while TP-060 MPL (30%) in Figure 2e presents a catalyst film. In both cases the catalyst coating may be considered homogenous in terms of catalyst distribution across the GDE surface, as identified by EDX (Figure S3). Also, no major catalyst agglomerates in the size range of the mean flow pore diameter were observed by SEM at low magnification (Figure S4). However, for the given catalyst loading of 2.0 ± 0.3 mg/cm^2, the catalyst layer neither bridges the open space in between the carbon fibers nor the cracks in the MPL. Figure 2c and f show (supported by EDX maps in Figure S3) that at least a good share of the deposited catalyst remains on the GDE surface. Moreover, the catalyst layer itself shows only minor topographical changes due to the electrochemical testing.

Figure 3, together with Videos S1–2, provides exemplary 3D-representations for the GDEs based on TP-120 (30%) and TP-120 MPL (30%) after the electrochemical testing, recorded by high-resolution X-ray computed tomography (XCT). In the 3D-representations, the location and spread of the catalyst can be determined due to the elemental contrast between C (grey) and Sn (yellow). From the comparison of the two GDEs, the depth penetration of the catalyst for the GDE based on TP-120 (30%) can be determined. The depth penetration is found to be much larger than for the GDE based on TP-120 MPL (30%). In fact, for the GDE based on TP-120 (30%) the catalyst layer appears to be smeared out, while the catalyst layer for the GDE based on TP-120 MPL (30%) appears to be focused to the GDE surface. At this, the focus holds for the whole MPL except for those parts, which are directly underneath the cracks in the MPL. This observation is in good agreement with previous findings for a study on SIGRACET GDLs for CO_2 electrolysis to CO. In this study, the MPL was found to support a focused structure of the catalyst layer as well.[35]

Table 2 reports the results of the contact angle (CA), porosity and through-plane conductivity measurements. In accordance with the SEM investigation, all three analyzes were performed for the pristine GDLs as well as the GDEs before and after the electrochemical testing. The CA-measurements in the pristine state of the GDLs provide that the electrode wetting by 1 M $KHCO_3$ for TP-060 and TP-120 (10%) is as high as about 141°. In contrast, TP-060 and TP-120 (30%) as well as TP-060 MPL and TP-120 MPL (30%) show CAs of about 144° and 146°, respectively. The higher CA of the latter four GDLs can be explained by their higher hydrophobic treatment as compared to TP-060 and TP-120 (10%). The slightly higher CA for TP-060 MPL and TP-120 MPL (30%) could be a result for the presence of the MPL.

Furthermore, Table 2 shows that the catalyst layer deposition impairs the hydrophobicity of the investigated samples as the CAs decrease for all samples. At this, the results for TP-060 MPL and TP-120 MPL (30%) show the most significant decrease with values in the range of 133°. The other samples show similar CAs in the range of 139°. The decrease of the hydrophobicity due to the catalyst layer deposition suggests

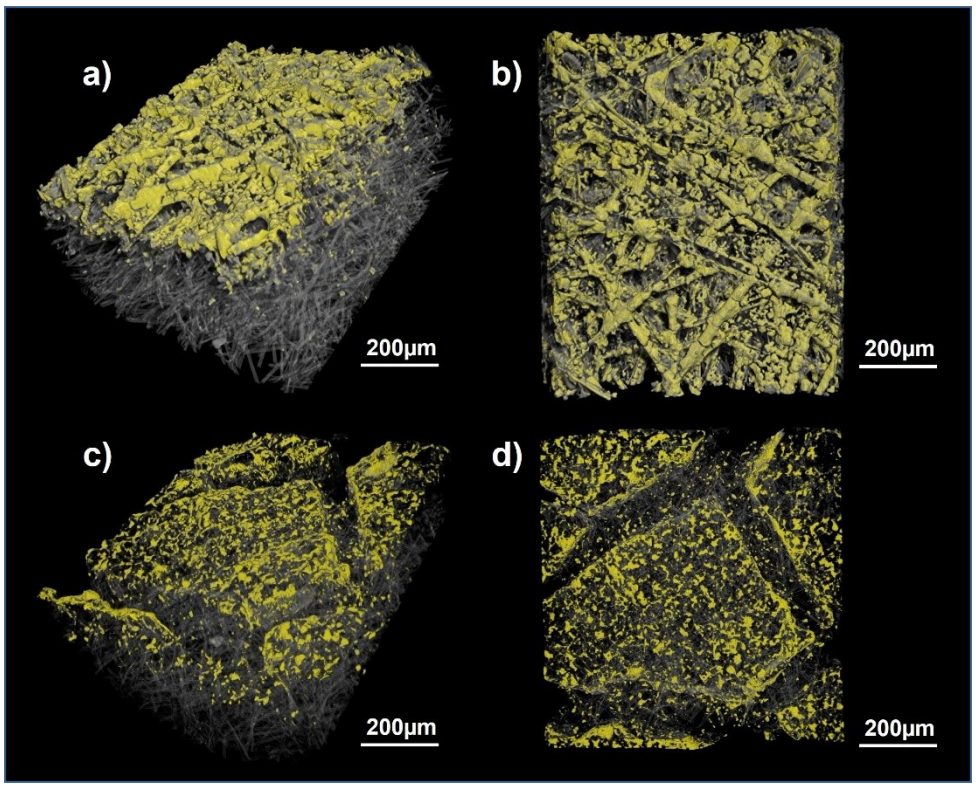

Figure 3. Exemplary XCT-images of the investigated gas diffusion electrodes (GDEs) after use. Yellow color indicates regions with high mass density, i.e., SnO_2 as a part of the catalyst layer vs. the carbon-based substrate. a–b) Side and top view for TP-120 (30%), c–d) Side and top view for TP-120 MPL (30%). (More details Video S1–2).

Table 2. Results for the contact angle, porosity, and through-plane conductivity measurements of the pristine GDLs as well as the GDEs before and after the CO_2 electroreduction. Contact angle measurements were performed using 1 M $KHCO_3$ electrolyte at room temperature. (Scattering of measurement results represents the standard deviation for contact angle and through-plane conductivity measurements and the estimated standard deviation for the mean flow pore diameter measurement (±10%)).

Gas Diffusion Electrode [GDE]	Contact Angle			Mean Flow Pore Diameter			Through-Plane Conductivity		
	GDL (pristine) [°]	GDE (before) [°]	GDE (after) [°]	GDL (pristine) [μm]	GDE (before) [μm]	GDE after) [μm]	GDL (pristine) [mS/cm]	GDE (before) [mS/cm]	GDE (after) [mS/cm]
TP-060 (10%)	141±6	140±4	41±12	29±3	27±3	28±3	6±3	0.00±0.3	0.5±0.2
TP-120 (10%)	142±8	138±7	42±20	25±3	24±2	30±3	10±2	0.02±0.02	3±1
TP-060 (30%)	143±4	141±11	44±14	26±3	25±3	31±3	5±1	0.0006±0.00002	5±2
TP-120 (30%)	145±4	139±3	42±11	23±2	23±2	22±2	18±13	0.04±0.06	13±0.9
TP-060 MPL (30%)	147±2	134±4	absorbed	23±2	23±2	24±2	7±0.6	0.06±0.01	0.4±0.2
TP-120 MPL (30%)	147±4	133±2	absorbed	22±2	25±3	24±2	11±1	0.2±0.2	2±0.4

that the hydrophobicity of the GDEs before the electrochemical testing is mostly governed by the hydrophobicity of Nafion in the catalyst layer. A reference experiment without catalyst nanoparticles showed that the deposition of Nafion alone reduces the CA of most samples even more (Table S1). Thus, the catalyst layer including Nafion appears to conceal the hydrophobicity of the GDL substrate. Moreover, the lower hydrophobicity for the GDEs based on TP-060 MPL and TP-120 MPL (30%) could be a result of the different surface topography as compared to the other GDEs without MPL. However, despite the rather stable surface topography as observed in Figure 2, the hydrophobicity of the GDEs is not constant over the course of the experiment after all. Table 2 provides that the hydrophobicity decreases significantly due to the electrochemical experiments. This is expressed by CAs of about 42° for the GDEs based on TP-060 and TP-120 (both 10% and 30%) and an immediately absorbed test liquid for the GDEs based on TP-060 MPL and TP-120 MPL (30%). The significant decrease of hydrophobicity could be a result for the (partial) displacement or deterioration of binder due to the electrochemical testing.[42] A similar behavior was observed for Nafion as a binder for fuel cell electrodes.[43] Furthermore, the difference in terms of wetting between the GDEs based on TP-060 MPL and TP-120 MPL (30%) as well as the other four electrodes could be related to the cracks in the MPL (Figures 2). In fact, the cracks might facilitate drainage of the electrolyte droplet. However, given the still existing hydrophobicity of the supporting carbon fibers and the MPL, the test liquid does not flood any of the electrodes.

Proceeding with the GDL porosity (Table 2), three out of four samples without MPL show a slight decrease of the mean flow pore diameter due to the catalyst deposition as well as an increase of the mean flow pore diameter due to electrochemical testing. For example, TP-060 (10%) shows a mean flow pore diameter of 29 μm in the pristine state, 27 μm after the catalyst deposition, and 28 μm after the electrochemical testing again. The slight decrease in mean flow pore diameter after the catalyst deposition suggests a slight reduction of the GDL porosity, which is expected due to the application of an additional layer. However, the catalyst deposition does not lead to clogged pores. This observation is supported by the SEM images in Figure 2. A continuous catalyst layer is not achieved for the given catalyst loading in this study. Furthermore, the increase of the mean flow pore diameter after the electroreduction suggests that the catalyst layer is removed from the GDE during the experiment. However, the finding of a removed catalyst layer is contradicted by the SEM images in Figure 2 and the EDX maps in Figure S3. The images show the presence of the catalyst layer even after the CO_2 electroreduction. Thus, the results of the mean flow pore diameter measurements do not provide strong evidence for a change of the electrode structure after all. The differences in terms of the absolute mean flow pore diameters are also quite small for some of the GDEs. Nevertheless, it is still interesting to observe that the mean flow pore diameters of the GDLs with MPL are very similar as compared to the GDLs without MPL despite the presence of a MPL with much smaller pores. For example, the mean flow pore diameter of TP-120 (30%) is as high as 23 μm and comparable to TP-060 MPL (30%), which shows a mean flow pore diameter of 23 μm, too. This result can be explained by the presence of cracks in the MPL as observed in Figure 2 that bypass the pores of the MPL. Thus, neither the catalyst deposition nor the electrode testing appear to affect the GDE porosity significantly (yet), while cracks in the MPL of TP-060 MPL and TP-120 MPL (30%) bypass the narrow pores of the MPL. However, porosity changes might still become relevant on longer time scales as observed for proton exchange membrane fuel cells (PEMFCs).[44]

Finally, the results of the electrical conductivity measurements in Table 2 provide that the through-plane conductivity of the investigated GDEs is highly dependent on the state of the electrodes. The state of the electrodes results from their preparation and utilization and may also be inhomogeneous as the experimental scattering for the through-plane conductivity measurements was found to be significant, particularly for the GDEs before use. Relating to this, the electrical conductivity of the pristine GDLs was found to be very similar for all samples in accordance with the hydrophobicity and the porosity. In all six cases the conductivity lies in a range from 5–18 mS/cm. Furthermore, Table 2 shows that the individual electrical conductivity of the GDEs before use is considerably lower as compared to the conductivity of the corresponding GDLs. The considerable decrease in conductivity can be explained by the deposition of an electrically insulting binder and oxidic catalyst particles on the GDE surface, i.e., Nafion and SnO_2. The vast

scattering on the other hand suggests a certain inhomogeneity of the binder and/or catalyst distribution across the carbon-based substrate. To be more specific, Table 2 shows that the through-plane conductivities decrease by at least two orders of magnitude due to the catalyst deposition and range from 0.6 μS/cm to 0.2 mS/cm afterwards. However, the insulating character of the catalyst layer is not maintained during the experiment. In fact, due to the repeated electroreduction the through-plane conductivities increase again. This could be a result for the reduction of SnO_2 to metallic Sn,[45] the (partial) displacement or deterioration of binder in line with the CA-observations, or both, as far as it is not visible to SEM. Following the evolution of the electrical conductivity of one GDE along its characterization, the GDE based on TP-060 (30%), for example, shows a conductivity of 5 mS/cm before the catalyst deposition, 0.6 μS/cm after the catalyst deposition and 5 mS/cm again after the electrochemical testing. Hence, the electrodes undergo significant change during the electrochemical experiments and the electrode conductivity cannot be considered constant throughout the experiment.

Electrochemical characterization

For the electrochemical characterization, the investigated GDEs were subjected to a specific, short-term investigation procedure that is schematically depicted in Figure S5. During the procedure, the GDEs were tested in three consecutive runs (Run 1–3) for CO_2 electroreduction to formate at constant cathodic current densities of −36, −71, and −107 mA/cm^2 (−100, −200 and −300 mA) in fresh 1 M $KHCO_3$ electrolyte for 45 min each. During each run, formate accumulated in the static electrolyte of the otherwise rapidly assembled cell set-up. The accumulation of the reaction product has negative feedback on the CO_2 conversion efficiency to formate given the pH sensitivity of the reaction.[46,47] Accordingly, in this study the Faradaic efficiency (FE) for CO_2-to-formate is compared for a fixed time interval at the beginning of each run (2–11 min after the electrolysis started). The procedure guarantees for largely comparable conditions during the individual runs for each GDE and allows for rapid conclusions regarding the effect of individual GDL properties on the GDE performance already.

Before and after each electrolysis run, PEIS- and LSV-scans were performed to determine the cathode-related part of the internal resistance of the cell setup and to monitor the evolution of the GDE performance in terms of cathodic current density. Table 3 provides the determined resistances derived from PEIS-scans at OCV as the first intersection of the impedance spectrum and the x-axis of the individual Nyquist-plots (Figure S6a). Looking at the results, the resistances decrease upon repeated use for each GDE. In fact, each experiment starts with the individually highest resistance before Run 1 and ends up with the individually lowest resistance before Run 3. This observation can be explained assuming an electrode conductivity[48] and/or electrode wetting[49] dependent contribution to the determined resistances in addition to a constant iR-drop across the electrolyte. To elucidate additional contributions to the internal resistance, a reference experiment using a silver sheet as a working electrode was performed. As a result, in accordance with literature, a constant and reproducible resistance of 0.7 Ω[39] was found for 1 M $KHCO_3$ (Figure S6b). This confirms the assumption of additional contributions to the internal resistance other than the iR-drop. However, a clear attribution is not directly possible since the hydrophobicity and electrical conductivity change simultaneously for all GDEs in this study (Table 2). In general, both an increased interface area as well as an improved electron transport in the electrode should lower the internal resistance for a non-ideal electrode.

Table 3. Results of the internal resistance measurement by PEIS as conducted prior to every electrolysis run (Figure S4) in fresh 1 M $KHCO_3$ at room temperature. (Standard deviation based on estimates (±10%)).

Gas Diffusion Electrode (GDE)	Area specific resistance R		
	Run 1 [Ω/cm^2]	Run 2 [Ω/cm^2]	Run 3 [Ω/cm^2]
Dioxide Materials (Reference)	0.42 ± 0.04	0.38 ± 0.04	0.38 ± 0.04
TP-060 (10%)	1.37 ± 0.1	0.61 ± 0.06	0.52 ± 0.05
TP-120 (10%)	1.32 ± 0.1	0.70 ± 0.07	0.56 ± 0.06
TP-060 (30%)	0.89 ± 0.09	0.61 ± 0.06	0.60 ± 0.06
TP-120 (30%)	0.69 ± 0.07	0.60 ± 0.06	0.53 ± 0.05
TP-060 MPL (30%)	0.50 ± 0.05	0.49 ± 0.05	0.49 ± 0.05
TP-120 MPL (30%)	0.51 ± 0.05	0.50 ± 0.05	0.49 ± 0.05

Looking into a couple of results in detail, Table 3 shows that the area specific resistances for the GDEs based on TP-060 MPL and TP-120 MPL (30%) slightly decrease from 0.51 and 0.50 Ω/cm^2 prior to Run 1 to 0.49 Ω/cm^2 for both prior to Run 3. Similarly, the other GDEs also show decreasing resistances, but feature higher overall values. For example, the GDE based on TP-120 (30%) shows 0.69 Ω/cm^2 prior to Run 1 and 0.53 Ω/cm^2 prior to Run 3, while the GDE based on TP-120 (10%) shows 1.32 Ω/cm^2 prior to Run 1 and 0.56 Ω/cm^2 prior to Run 3. Based on this, it may be assumed that the electrical through-plane conductivity has a larger effect on the determined resistances than the electrode wetting. This is because the resistances for the GDEs based on TP-060 MPL and TP-120 MPL (30%) reported in Table 3 start on a low level, with the through-plane conductivities being relatively high. The other GDEs on the other hand show high resistances for relatively low through-plane conductivities, for otherwise drastically decreasing hydrophobicities for both types of GDEs. In any case, the PEIS-measurements confirm a significant change of the GDE properties along with the electrochemical experiments. This was already expected based on the results in Table 2.

For further comparison, Table 3 also provides internal resistances for a commercial SnO_2-GDE by Dioxide Materials. This GDE shows the lowest of all resistances as well as a comparatively low decrease of the overall values, ranging from 0.42 Ω/cm^2 prior to Run 1 to 0.38 Ω/cm^2 prior to Run 3. The latter could be a result for the alternative GDE structure of the reference GDE. In case of the GDE by Dioxide Materials, the catalyst was mixed with carbon to create a mixed carbon/catalyst-layer instead.[50]

Figure 4 shows the evolution of the cathodic current density at −1.15 V_{RHE} (iR-drop corrected by 0.7 Ω) for the third of three LSV-scans prior to each CO_2 electroreduction run (complete LSV data shown Figures S7-8). Here, like the resistances from the PEIS-scans, the cathodic current density for most of the investigated GDEs decreases upon repeated use. For example, while the GDE based on TP-060 MPL (30%) shows a cathodic current density of −212.9 mA/cm^2 before Run 1, it shows only −178.7 mA/cm^2 before Run 2 and −148.1 mA/cm^2 before Run 3. However, while a deterioration of the GDE performance is expected due to potential degradation of GDE components,[42] a decline of the cathodic current density due to the electrochemical testing cannot generally be observed for all GDEs. As an exception, the reference GDE by Dioxide Materials shows a mostly stable, if not slightly increasing performance of −135.1 mA/cm^2 before Run 1, −141.9 mA/cm^2 before Run 2 and −119.7 mA/cm^2 before Run 3. This agrees with the largely stable cell voltage of a direct formic acid electrolyzer over several hundred hours at moderate current densities of −140 mA/cm^2 based on a similar cathode reported by Dioxide Materials.[51]

Furthermore, Figure 4 shows that the decrease of the cathodic current density at −1.15 V_{RHE} for the custom-made GDEs mostly occurs between Run 1 and Run 2. The performance before Run 2 and Run 3 on the other hand is mostly stable. For example, while the GDE based on TP-120 MPL (30%) shows a decrease of the cathodic current density by 31% from −203.2 mA/cm^2 before Run 1 to −139.8 mA/cm^2 before Run 2, it shows an identical performance comparing the results from before Run 2 and Run 3 (−140 mA/cm^2, each). Hence, the decrease of the cathodic current densities is mostly an initial effect that occurs along with the electrolysis in Run 1.

When relating the results of the LSV-scans to the results of the PEIS-measurements summarized in Table 3, it appears that a low initial internal resistance before Run 1 allows for a high cathodic current density in the following LSV-scan. This is suggested by the results for the GDEs based on TP-060 and 120 MPL (30%). Both samples show low initial resistances of 0.50 and 0.51 Ω/cm^2 as well as high cathodic current densities prior to Run 1, while the other four custom-made GDEs show higher resistances and, vice versa, lower cathodic current densities. However, given the parallel decrease of the electrode resistance and the cathodic current density for all GDEs, the suggested correlation does not hold for Run 2 and Run 3. Otherwise, the cathodic current densities of the GDEs should even increase for decreasing resistances, which is not the case. Thus, the change of the observed resistances in Table 3 cannot explain the loss in catalytic activity as observed in the LSV-scans. This suggests the presence of even more, potentially opposing, mechanisms behind the change of the GDE properties.

Concluding the present characterization, Figure 5 presents the results for the individual electrolysis runs of the investigated GDEs (Figure S9 reports the individual potential vs. time curves).

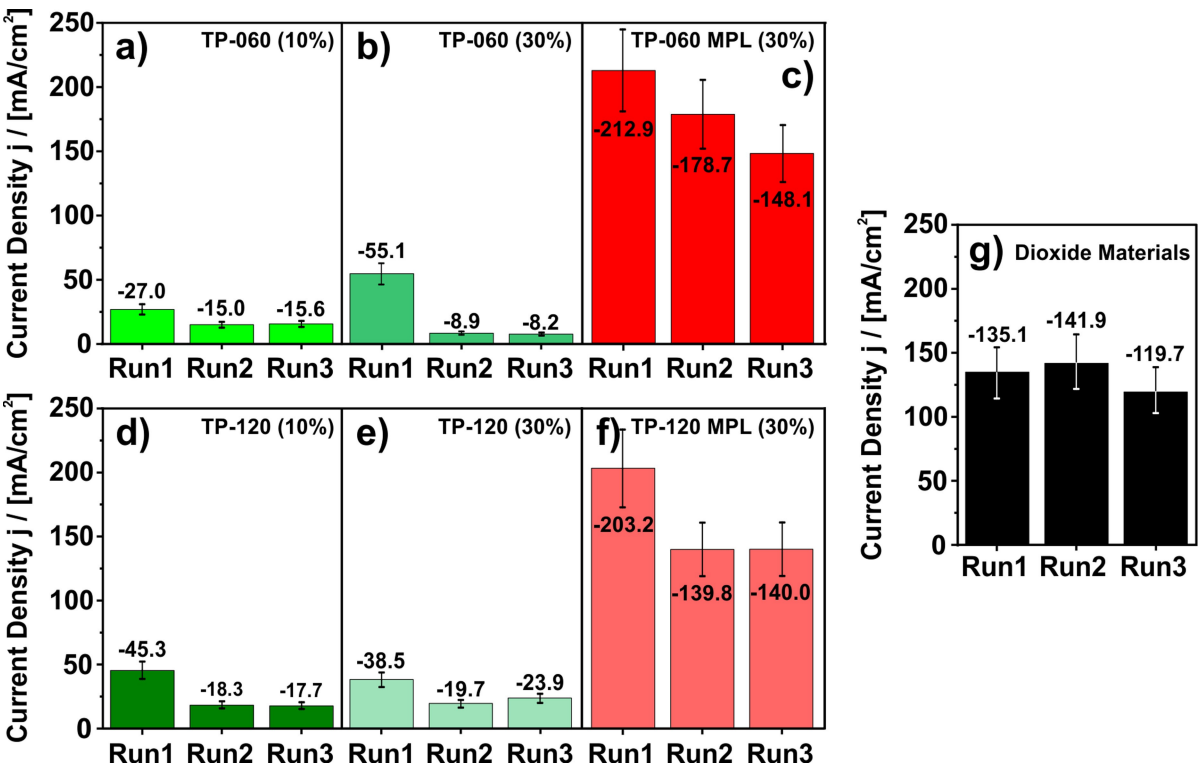

Figure 4. Evaluation of the current density at −1.15 V_{RHE} (iR-drop corrected) for the third of three LSV-scans prior to each electrolysis runs (Run 1–3). Results for the gas diffusion electrodes (GDEs) without microporous layer (MPL) are shown in green. Results for the GDEs with MPL are shown in red. The results for the reference electrode by Dioxide Materials is shown in black. (Additional details about the LSV-scans can be found in Figures S7–8. Error bars indicate the estimated standard deviation).

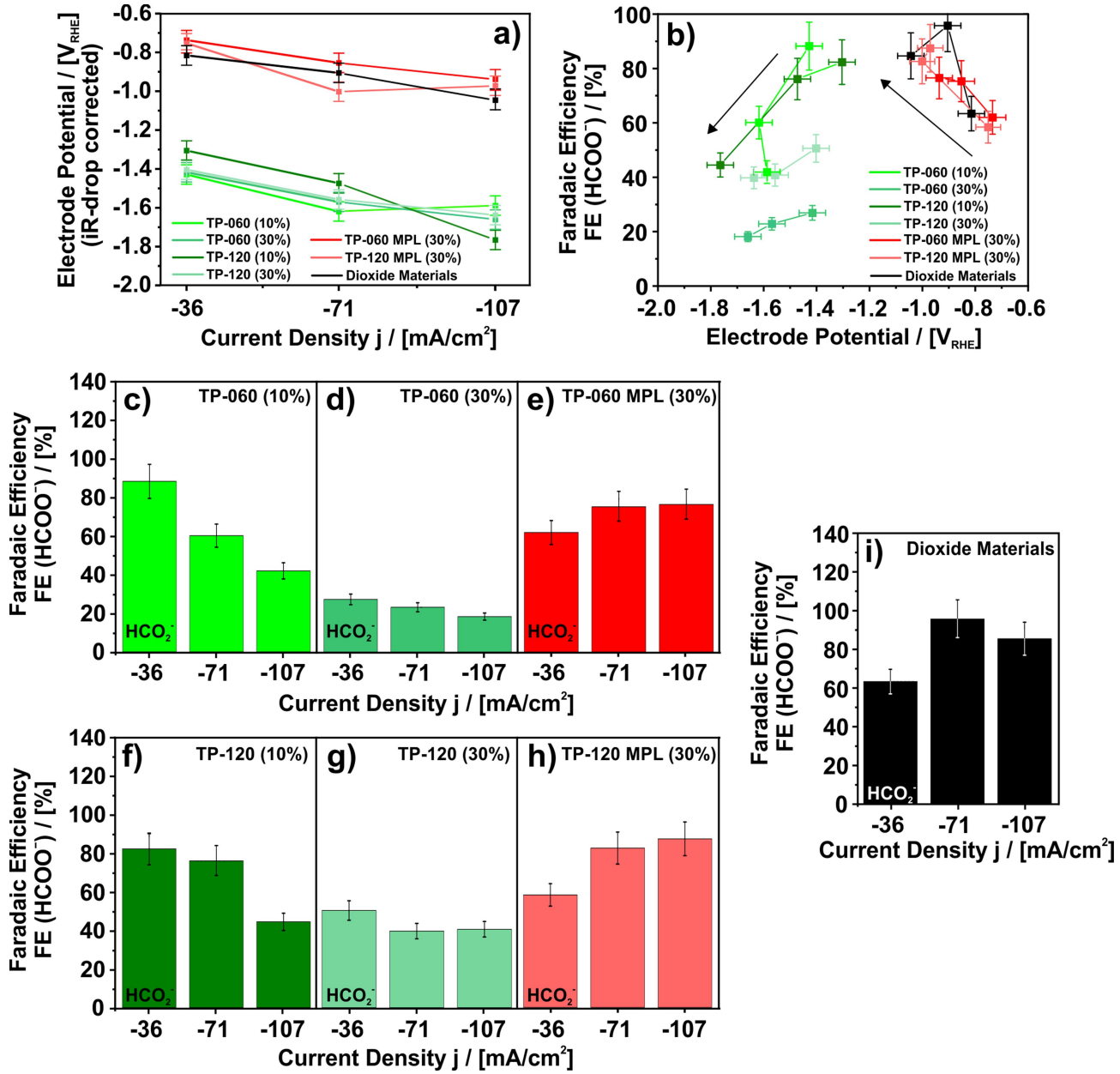

Figure 5. Evaluation of the average electrode potential and the resulting Faradaic efficiency FE for CO_2 electroreduction to formate at different current densities ranging from −36 to −107 mA/cm^2. Results for the gas diffusion electrodes (GDEs, cathodes) without microporous layer (MPL) are shown in green. Results for the GDEs with MPL are shown in red. The results for the reference electrode by Dioxide Materials are shown in black. a) Average electrode potential during 45 min of continous CO_2 electroreduction in 1 M $KHCO_3$. b) Average electrode potentials vs. corresponding FE for formate (Interval: 2–11 min). c–i) FEs for formate at different current densities ranging from −36 to −107 mA/cm^2 (Interval: 2–11 min) (Final concentration of formate shown in Figure S10. Error bars indicate the estimated standard deviation).

Figure 5a shows the average electrode potential of the GDEs (cathodes) during 45 min of continuous CO_2 electroreduction at constant cathodic current densities ranging from −36 mA/cm^2 to −107 mA/cm^2 −100 mA to −300 mA). As a general observation, the electrode potentials are getting more negative for an increasing cathodic current density. This is a direct result of the higher electrode polarization but is certainly affected by the GDE deterioration as observed via LSV already. For example, the GDE based on TP-060 (10%) shows an average electrode potential of −1.42 V_{RHE} at −36 mA/cm^2 and −1.59 V_{RHE} at −107 mA/cm^2.

Furthermore, the results for the average electrode potential during the electrolysis in Figure 5a can be divided into two groups. For group 1 the electrode potentials are always more negative than −1.2 V_{RHE}. For group 2 the electrode potentials are always more positive than −1.2 V_{RHE}. Within the individual groups, neither major nor consistent differences become apparent. For example, while the GDE based on TP-120 (10%) shows the most positive electrode potential for −36 and

−71 mA/cm² with −1.31 V_{RHE} and −1.4 V_{RHE} in group 1, it shows the most negative electrode potential at −107 mA/cm² with −1.77 V_{RHE}. Similarly, in group 2, a consistent trend regarding an advantage for any of the three GDEs is not apparent either. At −36 mA/cm² the electrode potentials lie in a range from −0.74 V_{RHE} to −0.81 V_{RHE}, while at −107 mA/cm², the electrode potentials lie in a range from −0.94 V_{RHE} to −1.05 V_{RHE}.

Figure 5c–i displays the FE for the electroreduction of CO_2 to formate corresponding to the measurements summarized in Figure 5a. Here, as a general observation, the Faraday efficiency for the evolution of formate shows a broad range spanning from 18 to 96%. The remaining charge is consumed by HER or CO_2 electroreduction to CO (Figure S11). For the electroreduction to formate, the results can be divided into the same two groups as for the average electrode potential. The first group of GDEs shows a mostly decreasing FE, while the second group shows a mostly increasing FE for an increasing cathodic current density. Accordingly, in group 1 the GDE based on TP-060 (10%) shows the highest FE of 88% at −36 mA/cm² and 42% at −107 mA/cm², while the GDE based on TP-120 (10%) shows the highest FE of 76% at −71 mA/cm². In group 2, overall, the reference GDE by Dioxide Materials shows the highest FE of 96% at −71 mA/cm², while the GDE based on TP-120 MPL (30%) provides a FE of 87% at −107 mA/cm².

Combining the results from Figure 5a and Figure 5c–i, Figure 5b provides a representation showing the FE for the conversion of CO_2 to formate in dependency of the average electrode potential during the electrolysis. In the resulting plot, the investigated GDEs show the best CO_2 conversion at around -1.2 ± 0.2 V_{RHE}, with a tendency to increasing FEs from −0.8 to −1.1 V_{RHE} and decreasing FEs for electrode potentials more negative than −1.3 V_{RHE}. Accordingly, TP-060 and 120 (10%) show a decreasing FE, while TP-060 and 120 MPL (30%) show an increasing FE for an increasing cathodic current density each. Thus, the efficiency for the CO_2 electroreduction to formate for the investigated GDEs is highly electrode potential dependent, while the electrode potential must neither be too positive nor too negative to allow for an efficient conversion. This observation corresponds well with previous reports, where medium electrode potentials of −1.2 V_{RHE},[52] −1.14 V_{RHE}[53] and −1.10 V_{RHE}[54] have been identified as the most efficient potentials for CO_2-to-formate on Sn-based catalysts as well.

Effect of the GDL Thickness

In the present study the results for the GDE performance do not show specific differences to render a preferential decision for any of the two investigated GDL thicknesses, although thinner GDLs can be expected to provide lower electrical resistances. Particularly in terms of FE towards formate shown in Figure 5, the results show variable advantages for both types of GDEs. For example, while the GDE based on TP-060 (10%) shows a slightly higher FE for formate at −36 mA/cm² than the GDE based on TP-120 (10%) with FE = 88% vs. 82%, the GDE based on TP-120 (30%) outperforms the GDE based on TP-060 (30%) for the same cathodic current density with FE = 50% vs. 82%. Furthermore, also the LSV results are largely identical in terms of the observed cathodic current densities. For example, the GDE based on TP-060 (10%) shows current densities of −15.0 and −15.8 mA/cm² in Run 2 and Run 3, which is comparable to the GDE based on TP-120 (10%) with −18.3 and −17.7 mA/cm² after identical pretreatment. The similarity for the GDE performance depending on the GDL thickness is explained by the mostly identical GDE properties as identified by microscopy images, contact angle (CA)-, porosity-, through-plane conductivity- and PEIS-measurements. In fact, the imaging techniques revealed no influence for the GDL thickness on the GDE surface morphology, which is an expected result since the bulk material is not involved in the GDE preparation. Similarly, the CA- and the porosity measurements did not provide any discernible difference, due to the exclusive surface sensitivity of the CA-measurements and the homogeneity of the GDL fiber structure (Video S1). Furthermore, the PEIS-measurements did not show any advantage for thin over thick GDEs either, although higher resistances for thicker GDEs have to be expected, due to longer conductive pathways for thicker GDLs.[55,56] On the contrary, the GDE based on TP-060 (30%) shows an even higher resistance of 0.60 Ω/cm² before Run 3 than the GDE based on TP-120 (30%) with 0.53 Ω/cm² (Table 3). The latter is in accordance with the through-plane conductivity, which is higher for the GDE based on TP-120 (30%) than for the GDE based on TP-060 (30%), 13 mS/cm² vs. 5 mS/cm². However, as apparent for the other GDE couple without MPL, the through-plane conductivity cannot be treated as a single descriptor to predict the internal resistance as observed by PEIS. In fact, although the GDE based on TP-060 (10%) shows a lower through-plane conductivity than the GDE based on TP-120 (10%), 0.5 vs. 3 mS/cm², the observed resistance in the PEIS-scan before Run 3 is lower too, 0.52 vs. 0.56 Ω/cm². Thus, a supporting effect of the Toray Paper thickness for the CO_2 electroreduction towards formate is not observed. With this, the present results are in very good agreement with previous results for a study on the effect of the GDL thickness on the electrode performance in a proton exchange membrane fuel cell (PEMFC), where no direct correlation for the thickness and the electrode performance was found as well.[57] Similarly, in a recent study for CO_2-to-CO, the GDL thickness had no effect on the GDE performance during short-term measurements. Only during long-term measurements (> 100 h), GDEs based on thicker GDLs had an advantage over thinner ones.[37] A possible reason for this was given in a study for CO_2-to-formate, where thicker GDLs, driven by custom-made MPLs with increasing thickness, showed better performance than thinner ones, due to the extended prevention of pore flooding.[58] On the contrary, it has also been reported that an increased GDL thickness may affect the GDE performance negatively, due to decreased transport rates of CO_2.[36] However, the transport limit certainly requires a comparatively high current density to become effective, which is not the case for the present study.

Effect of the Hydrophobic Treatment

Unlike the GDL thickness, the PTFE content of the substrate does influence the electrochemical performance of the investigated GDEs in the absence of an MPL. This is an expected result since the electrode wetting determines the extent of the CO_2 electroreduction at the GDE/electrolyte interface.[33] When the results of the GDEs based on TP-060 and 120 (10%) and the GDEs based on TP-060 and 120 (30%) are compared, a lower hydrophobic treatment of the GDL appears to be beneficial for the FE of the CO_2 electroreduction to formate. For example, the GDE based on TP-060 (10%) shows FEs of 88% at -36 mA/cm^2, 57% at -71 mA/cm^2, and 42% at -107 mA/cm^2, while the GDE based on TP-060 (30%) shows only 27% at -36 mA/cm^2, 23% at -71 mA/cm^2, and 18% at -107 mA/cm^2 (Figure 5). However, the current trend for a better GDE performance in terms of selectivity for a lower hydrophobic treatment is not met by the results for the LSV-scans in Figure 4. Here, the LSV-scans show very similar results for both GDE pairs without MPL.

A suitable explanation for the observed advantage of the GDEs based on Toray Paper (10% PTFE) is challenging. In fact, the CAs, the porosity, and the electrical conductivity of the pristine GDEs without MPL were found to be very similar regardless the hydrophobic treatment (Table 2). For example, while the GDE based on TP-060 (10%) showed a CA of 139.8° before and 41.1° after the electroreduction of CO_2, the GDE based on TP-060 (30%) showed a CA of 140.9° before and 43.5° afterwards. Therefore, the interface between the catalyst, the electrolyte and the gas phase should be mostly identical for both types of GDEs, governed by the composition of the catalyst layer. Furthermore, the unexpectedly lower electrical through-plane conductivities for the GDEs based on Toray Paper (10% PTFE) after the electrochemical testing[59] do apparently not affect the electrode performance negatively. The only major difference depending on the hydrophobic treatment was the initial internal resistance as observed by PEIS. Here, the internal resistance was significantly higher for the GDEs based on Toray Paper with 10% PTFE (1.37 and 1.32 Ω/cm^2, Table 3) as compared to the GDEs based on Toray Paper with 30% PTFE (0.89 and 0.69 Ω/cm^2). Moreover, the internal resistances for the former also decreased more significantly during the electrochemical characterization than the internal resistances for the latter. This suggests a more significant change for the properties of the former along with the electrochemical testing than for the latter.

Comparing the present results with literature, both agreement and disagreement with previous studies can be found. For the agreeing part, in a study for the effect of the carbon fiber substrate on the performance in the electrochemical reduction of CO_2 to CO, a low hydrophobic treatment of 10% PTFE was found to provide the best performance in terms of partial current density as well.[34] For the disagreeing part, in a study for the effect of the hydrophobic treatment on the electrode performance in a proton exchange membrane fuel cell (PEMFC), superior performance was observed for GDEs based on GDLs with the highest amount of PTFE.[57] Furthermore, also in a recent study for CO_2-to-CO no significant effect of the hydrophobic treatment of the GDL on the selectivity of the electroreduction was observed in the absence of an MPL.[37] Both is the opposite of the present findings. However, the disagreement may be explained by the different use cases. In the study for PEMFCs the cathode was investigated in a membrane electrode assembly (MEA), where the reaction product, water, had to be released with the outlet gas on the backside of the GDE. Similarly, also in the study for CO_2-to-CO, the reaction product, CO, had to be released from the GDE backside. In the present setup, however, the release of formate towards the liquid electrolyte on the front-side of the GDE is desired.

Effect of the Microporous Layer (MPL)

Considering the results of the present study, the presence of an MPL is of marked importance for the GDE performance. Particularly in terms of the cathodic current density, the presence of an MPL increased the GDE performance by a factor of up to 18 as compared to GDEs without MPL. For example, the GDE based on TP-060 MPL (30%) showed a cathodic current density of -148.1 mA/cm^2 in Run 3, while the GDE based on TP-060 (30%) showed only -8.2 mA/cm^2 for the same electrode potential (Figure 4). In turn, the higher cathodic current densities allow for higher product concentrations in the electrolyte (Figure S10) or, vice versa, lower electrode potentials for a certain current density (Figure 5a). However, considering the FE, the performance of a GDE with MPL may not outperform a GDE without MPL at any rate. In fact, as indicated by Figure 5b, the FEs for the GDEs based on Toray Paper appear to show an optimum around -1.2 V_{RHE}, which is yet to be achieved by even higher cathodic current densities for GDEs with MPL.

In general, the significantly improved performance of GDEs with MPL as compared to GDEs without MPL may have several reasons. These are the altered electrode wetting, better electrical connectivity of the catalyst and improved CO_2 distribution in the GDE. As a reason for the better performance of GDEs with MPL in this study, it can, firstly, be concluded that the MPL acts as a physical barrier for the catalyst nanoparticles upon deposition as identified by XCT. With this, the MPL leads to a focused catalyst layer on top of the GDE surface (Figure 6a), in good contact with the electrolyte (Figure 6b). This is contrary to GDEs without MPL where the open structure of the GDL allows for deep penetration of the catalyst nanoparticles into the inner GDL volume (Figure 6c). In the inner GDL volume, the catalyst nanoparticles can be considered partially out of reach for the electrolyte (Figure 6d).

The present finding is in good agreement with a previous study for the effects of the MPL on electrolyte flooding and the selectivity of CO_2 electrolysis to CO.[35,37] In the first study, Ag-particles were found to be focused to the GDE surface in the presence of an MPL, while GDLs without MPL allowed for deeper penetration of the catalyst particles in the carbon fiber support.[35]

Secondly, a comparatively low hydrophobicity, as observed by the CA-measurements after the electroreduction (Table 2)

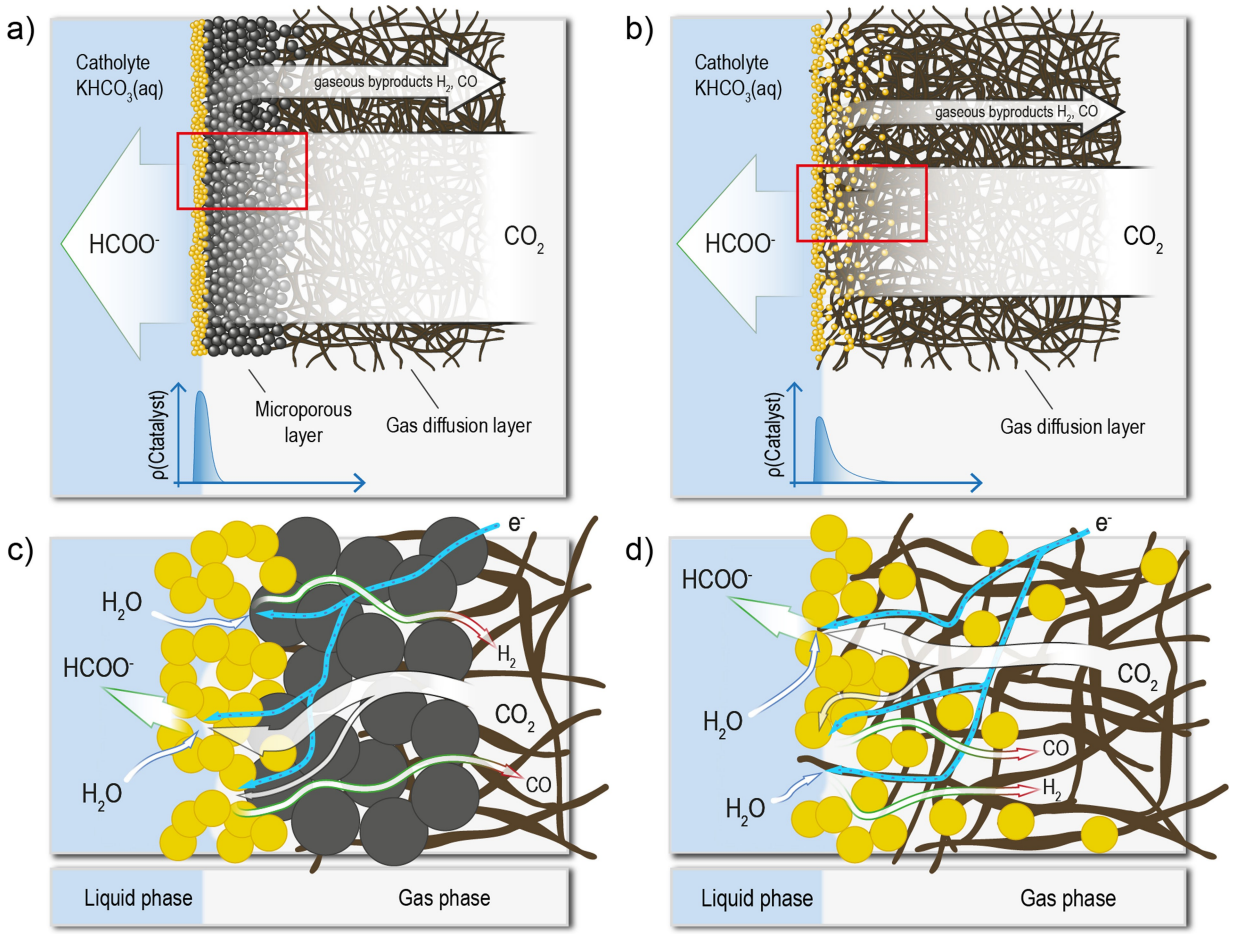

Figure 6. Schematic illustration or the reaction conditions on the investigated gas diffusion electrodes (GDEs) in this study. a) GDE with microporous layer (MPL) that leads to a focused catalyst layer on the GDE surface. b) GDE without MPL, thus, missing physical barrier for the catalyst nanoparticles (SnO_2, shown yellow) during the GDE manufacturing. c) Detailed schematic for the reaction interface of a GDE with MPL and a catholyte. (Most catalyst nanoparticles are in contact with the catholyte.) d) Detailed schematic for the reaction interface of a GDE without MPL and a catholyte. (In this case, some nanoparticles are lost for the reaction since they are not in contact with the catholyte.)

can be considered beneficial for the GDEs as well. A low hydrophobicity allows for a complete wetting of the catalyst layer, which would enhance the extent of the CO_2 electroreduction, in case a catalyst loading close to optimum is met.[60] However, it also appears possible, that the GDE performance in terms of current density or FE($HCOO^-$) could be even higher, if the electrodes maintain their initial hydrophobicity.

Furthermore, in Table 2 it was shown that the GDEs with MPL before the electrochemical testing show an electrical conductivity that is about one order of magnitude higher than the conductivity for the GDEs without MPL. The latter supports lower electrode potentials for a given current density in accordance with previous findings in literature.[61] However, a vast difference between the through-plane conductivity for the GDEs with and without MPL could only be retrieved for the pristine state and is overturned due to the apparent changes of the GDEs during the electrochemical reduction of CO_2. The presumed advantage for the GDEs with MPL in terms of electrical connectivity between the catalyst and the GDL is only apparent in the PEIS-measurements (Table 3). Here, the GDEs based on TP-060 and 120 MPL (30%) start with comparatively low internal resistances of 0.50 and 0.51 Ω/cm^2 and decrease just slightly to 0.49 Ω/cm^2 each.

Evaluating the present results, vast agreement for the significantly better performance of GDEs with MPL as compared to GDEs without MPL is found in literature.[34,35,37] For example, in the study for the effects of the MPL on electrolyte flooding and the selectivity of CO_2 electrolysis to CO, the GDEs with MPL were found to outperform GDEs without MPL clearly. This particular difference was associated with the flooding of the GDEs without MPL.[35] Similarly, a limited conversion efficiency towards CO was also observed in a previous study with different substrates, where a limited partial current density towards CO in the absence of an MPL was observed, too.[34] Furthermore, in the third study, the CO_2 electroreduction to CO was found to be enhanced, while the HER was the predominant reaction in the absence of an MPL.[37]

Thus, the present results agree with previous findings and extend the existing knowledge by a dedicated study for CO_2-to-formate. As a matter of fact, the present results follow similar trends in terms of optimum GDL choice, although the impact differs depending on the target product.[32] Unlike

previous studies,[58] even the GDEs without MPL allowed for extended testing under the given experimental conditions without flooding. During these tests the GDEs still provided a decent amount of product, at the cost of a higher electrode potential.

Conclusion

In the present study six commercial gas diffusion layers (GDLs) differing in the presence of a microporous layer (MPL), the GDL thickness, and the extent of the hydrophobic treatment, were investigated for their influence on the CO_2 electroreduction to formate. The investigation was performed in a static, gas-fed electrolysis setup specifically designed for the investigation of gas diffusion electrodes (GDEs). It was shown that the presence of an MPL improves the cathodic current density and the Faradaic efficiency for CO_2-to-formate significantly. The Faradaic efficiency was found to increase for an increasing cathodic current density at least up to -107 mA/cm^2 and was as high as 87% using SnO_2 nanoparticles as a catalyst. Other than the MPL, the extent of the hydrophobic treatment proved to be of some importance in the absence of an MPL, with 10% allowing for better GDE performance than 30% PTFE treatment. The GDL thickness, on the other hand, did not prove to be influential in the applied setup at all. Thus, aiming for maximum amounts of formate, GDLs with MPL should be employed as a GDE substrate to advance its performance, e.g., in terms of the maximum cathodic current density, beyond state-of-the-art electrodes. Here, the reason for the superior performance of GDEs with MPL lay in a decent combination of a focused catalyst layer, as identified by high-resolution X-ray computed tomography, the wetting, and the electrical conductivity. Furthermore, it was observed that all GDEs undergo significant change in terms of wetting and conductivity during the initial electrochemical testing. However, the changes on the GDE did not immediately manifest in the surface topography of the catalyst layer.Therefore, no electrochemical conversion of the catalyst and/or the (partial) displacement or deterioration of the binder is indicated.

Experimental Section

Gas diffusion electrode preparation

For the preparation of the investigated gas diffusion electrodes (GDEs), various gas diffusion layers (GDLs, Table 1, FuelCell Store, USA) were cut into 3×3 cm pieces. A catalyst ink consisting of SnO_2 nanoparticles (33 mg, nanopowder (particle size: <100 nm, broad range of 10–80 nm[38]), Sigma Aldrich, Germany), Nafion resin solution (23 µl, 15 wt% in H_2O/EtOH, IonPower, Germany) and isopropyl alcohol (3 ml, ROTIPURAN $\geq$99.8%, p.a., Roth, Germany) was prepared by ultrasonication for 30 min. The catalyst ink was deposited on the GDLs via manual spray coating with an airbrush (HG Trigger type 0.3 mm Double Action, Tamiya, Japan), resulting into a homogeneous catalyst loading of about 2.0 ± 0.3 mg/cm^2.

The reference electrode 'Dioxide Materials' was purchased from Dioxide Materials (USA). The properties of the custom-made GDE were as follows according to the manufacturer[50]: catalyst material (SnO_2 nanoparticles), catalyst loading (4 mg/cm^2), gas diffusion layer (GDL, Toray Paper TGP-H-120 (50% PTFE)), catalyst layer composition (150 mg catalyst, 150 mg Vulcan carbon XC72, 240 µl Sustainion XA-9 ionomer solution as a binder, dispersed in 1 ml water in 25 ml ethanol, spray coated onto GDL). The GDE was used without further pretreatment.

Materials characterization

The investigation of the GDE topography was performed with a scanning electron microscope (SEM, Quanta FEG 650 ESEM, FEI, The Netherlands) coupled with an energy dispersive X-ray detector (EDX, Octane Super-A, Ametek, USA). The EDX detector was implemented to visualize the catalyst distribution across the GDE surface. 3D images of the GDEs were acquired by high-resolution X-ray computed tomography (XCT, Xradia Versa 620, Zeiss, Germany).

The sessile drop contact angles of 1 M $KHCO_3$ in air were recorded on an optical contact angle goniometer (OCA100, DataPhysics Instruments, Germany). For the measurement, 2 µl droplets were dispensed onto three different locations of every sample, determining an average contact angle. Each sample was thoroughly rinsed with deionized water and dried in air to remove residual electrolyte before the measurement.

The determination of the mean flow pore diameter was implemented with a capillary flow porometer (Porometer 3GzH, ex Quantachrome - now 3P Instruments, Germany), using the liquid expulsion technique. For this, a wet- and a dry run were performed. Before the wet run, both circular-shaped samples of the GDLs and the GDEs which were punched-out from a larger specimen were immersed in a wetting fluid to fill the pores of the sample (Porofil, ex Quantachrome – now 3P Instruments, Germany). For the investigation of the GDEs after the electrochemical testing, the circular-shaped samples were taken from the electrolyte-exposed and uncompressed electrode area only.

The electrical conductivity was determined with a multimeter attached to the conductive tips of a foil thickness gauge (Figure S12, Käfer, W&Z-Vertrieb, Germany). The resulting electrical through-plane resistance as well as the thickness of the samples was determined for a mechanical load of 12 kPa. Based on these two values, the electrical through-plane conductivity was calculated for a contact area of 50 mm^2.

Electrochemical measurements

The electrochemical analyzes of the GDEs was performed in a commercial, gas-fed, three-electrode PTFE batch reactor (Figures S13–14, FlexCell PTFE, Gaskatel, Germany).[62] The electrochemical measurements were performed using a multichannel potentiostat (VSP-300, BioLogic, France). The GDEs were used as the working electrodes (WEs), a coiled Pt wire was used as the counter electrode (CE, Gaskatel, Germany) and an Ag/AgCl electrode was used as the reference electrode (RE, RE-1CP, ALS, Japan). The active electrode area, i.e., the cathode area exposed to the electrolyte, was 2.81 cm^2. 1 M $KHCO_3$ (ACS Reagent, $\geq$99.7%, Fluka Honeywell, Fisher Scientific, Germany) was used for both catholyte and anolyte, respectively, starting every measurement at room temperature. The catholyte volume was 12 ml. The anolyte volume was 30 ml. The two compartments of the cell were separated by a Nafion 117 membrane (IonPower, Germany), which was stored in DI-water without extensive pretreatment. During the electrochemical measurements, a continuous CO_2 flow (99,995%, Air Products, Germany)

of 20 sccm was applied to the cell, controlled by a mass flow controller (EL-FLOW, 10 ml to 500 ml, Bronkhorst, The Netherlands). All measurements were conducted at room temperature.

The electrochemical analysis was carried out according to a specific procedure, which is schematically depicted in Figure S5. Each GDE was investigated at three different current densities (Run 1: -36 mA/cm^2, Run 2: -71 mA/cm^2 and Run 3: -107 mA/cm^2) for 45 min per electrolysis run. Prior to each run a "before" measurement sequence was conducted, consisting of a potentiostatic electrochemical impedance spectroscopy (PEIS-) measurement, three cyclic voltammograms (CVs, in a range from OCV to -0.8 $V_{Ag/AgCl}$) and three repetitive linear sweep voltammetry scans (LSV-scans, from OCV to -2.0 $V_{Ag/AgCl}$). The LSV-scans were repeated three times to ensure experimental stability. For the comparison between the different GDEs, only the last scan is used. Furthermore, after each run an "after" measurement series followed, consisting of a PEIS- and three LSV-scans. Moreover, in between Run 1 and Run 2 as well as in between Run 2 and Run 3, the electrolyte was exchanged and refreshed manually, providing comparable starting conditions for each of the three runs.

All potentials in this paper are reported with reference to the Reversible Hydrogen Electrode (RHE), recalculating the potential of the RE according to the following equation 1 and assuming a constant pH of the CO_2 saturated electrolyte (1 M $KHCO_3$) of pH = 7.6.

$$E(RHE) = E(Ag/AgCl) + 0.059\,V \cdot pH + 0.210\,V \quad (1)$$

Product analysis

For the quantification of the evolving products, online gas chromatography (GC, Trace 1310, Thermo Scientific, USA) and offline ion exclusion chromatography (IC, S150, Sykam, Germany) were applied. The GC system was equipped with two channels using a sequence of a Haysep Q, a Molecularsieve 5 Å packed column and a thermal conductivity detector, each. For for the determination of H_2 and CO, Ar (6 N, Linde, Germany) or He (6 N, Air Products, Germany) was used as a carrier gas, respectively. Sample acquisition took place every nine minutes: automatically via a transfer line for the gaseous products and manually, by collecting 0.5 ml samples of catholyte for the determination of formate (without refill of fresh electrolyte). For quantification both methods were calibrated using external standards. For the gas products, H_2 and CO, calibration measurements with certified calibration gases (Linde, Germany) were conducted (3-point calibration with fixed amounts of H_2 (1000 ppm, 16700 ppm, 99700 ppm) and CO (979 ppm, 19900 ppm, 99900 ppm)). The gas flow out of the cell was determined prior to every measurement with a gas counter (MGC-1V3.4 PPMA, MilliGascounter, Ritter, Germany). The flow was determined three times and the average was used for the calculation of the Faradaic efficiency (FE). FE_{H2} and FE_{CO} were calculated as a momentary value using the following equation 2:

$$FE_i = \frac{z_i \cdot F \cdot \frac{p}{R \cdot T} \cdot V_{out} \cdot c_i}{I} \cdot 100\,\% \quad (2)$$

Here, z denotes the number of electrons transferred (= 2), F denotes Faraday's constant, p denotes the outlet pressure 1.013 bar, R denotes the universal gas constant, T denotes the temperature, V_{out} denotes the flow rate of the eluent gas, c_i denotes the determined product gas concentration and I denotes the total applied current.

The IC system was equipped with a SykroGel-Ex 450 SA-E01 column using an aqueous eluent solution comprising 7% acetonitrile ($\geq$ 99.3%, HiPerSolv CHROMANORM, VWR, USA) and 0.7 mmol perflourobutyric acid (99%, Thermo Scientific, USA). Prior to each analysis run of multiple samples, a calibration series in a range from $3.3 \cdot 10^{-4}$ mol/L to $2.2 \cdot 10^{-2}$ mol/Lwas recorded.

Comparing the concentration of formate in the static catholyte of the cell, the Faradaic efficiency (FE) for the electroreduction of CO_2 to formate was calculated as an interval value ΔFE, using the following equations 3–5:

$$\Delta FE = \frac{Q_{theo\,(x+1)} - Q_{theo(x)}}{Q_{tot(x+1)} - Q_{tot(x)}} \quad (3)$$

$$Q_{theo} = n \cdot z \cdot F \cdot 0.277 \quad (4)$$

$$Q_{tot} = \Sigma\,(I \cdot t) \quad (5)$$

Here, Q_{theo} denotes the theoretical charge, which was determined based on the produced amount of formate during a certain time interval x and Q_{tot} denotes the total charge measured during the individual experiment.

With respect to GDE reproducibility, the preparation and electrochemical analysis of one GDE was repeated three times. Based on the scattering of the individual results for these three measurements in terms of Faradaic efficiency for formate, H_2 and CO as well as the electrode potential during LSV, the electrode potential during continuous electroreduction of CO_2 to formate, the internal area specific resistance determined by PEIS and the mean flow pore diameter the standard deviation was estimated conservatively. The estimated standard deviations are as follows and were added as error bars to the corresponding results:

LSV current density: ± 15% on the reported value

Faradaic efficiency – Formate: ± 10% on the reported value

Faradaic efficiency – H_2: ± 33% on the reported value

Faradaic efficiency – CO: ± 50% on the reported value

Mean electrode potential: ± 0.05 V_{RHE} on the reported value

Mean flow pore diameter: ± 10% on the reported value

Area specific internal resistance: ± 10% on the reported value

Acknowledgements

The authors kindly acknowledge the financial support from the German Federal Ministry of Education and Research within the project 'iNEW2.0 - Inkubator Nachhaltige Elektrochemische Wertschöpfungsketten' Project No. 03SF0627A.. The authors thank Sebastian B. C. Lehmann for the contributions in graphical design and Henrike Gattermann for language editing.

Conflict of Interests

The authors declare no conflict of interest.

Data Availability Statement

The data that support the findings of this study are available from the corresponding author upon reasonable request.

Keywords: Power-to-X · CO_2 electroreduction · formate · gas diffusion electrode · Toray Paper

[1] World Meteorological Organization - Provisional State of the Global Climate 2022, Genf, **2022**.
[2] S. Boehm, L. Jeffery, K. Levin, J. Hecke, C. Schumer, C. Fyson, A. Majid, J. Jaeger, A. Nilsson, S. Naimoli, J. Thwaites, E. Cassidy, R. Waite, R. Wilson, S. Castellanos, N. Singh, A. Lee, A. Geiges, *State of Climate Action 2022*, Washington D. C., **2022**.
[3] A. Al-Mamoori, A. Krishnamurthy, A. A. Rownaghi, F. Rezaei, *Energy Technol.* **2017**, *5*, 834–849.
[4] S. M. Jordaan, C. Wang, *Nat. Catal.* **2021**, *4*, 915–920.
[5] J. Burre, D. Bongartz, L. Brée, K. Roh, A. Mitsos, *Chemie Ing. Tech.* **2020**, *92*, 74–84.
[6] B. Rego de Vasconcelos, J.-M. Lavoie, *Front. Chem.* **2019**, *7*, Article 392.
[7] R. Eichel, W. Leitner, K. Wagemann, *Chemie Ing. Tech.* **2020**, *92*, 3–3.
[8] D. L. T. Nguyen, Y. Kim, Y. J. Hwang, D. H. Won, *Carbon Energy* **2020**, *2*, 72–98.
[9] M. Löffelholz, J. Osiewacz, A. Lüken, K. Perrey, A. Bulan, T. Turek, *Chem. Eng. J.* **2022**, *435*, 134920.
[10] M. Quentmeier, B. Schmid, H. Tempel, H. Kungl, R.-A. Eichel, *ACS Sustain. Chem. Eng.* **2023**, *11*, 679–688.
[11] S. R. Foit, I. C. Vinke, L. G. J. de Haart, R.-A. Eichel, *Angew. Chemie Int. Ed.* **2017**, *56*, 5402–5411.
[12] Y. Hori, *Mod. Asp. Electrochem.* (Eds.: C. G. Vayenas, R. E. White, M. E. Gamboa-Aldeco), Springer Science + Business Media, New York, **2008**, pp. 89–189.
[13] A. S. Agarwal, Y. Zhai, D. Hill, N. Sridhar, *ChemSusChem* **2011**, *4*, 1301–1310.
[14] M. F. Philips, G.-J. M. Gruter, M. T. M. Koper, K. J. P. Schouten, *ACS Sustain. Chem. Eng.* **2020**, *8*, 15430–15444.
[15] S. A. Al-Tamreh, M. H. Ibrahim, M. H. El-Naas, J. Vaes, D. Pant, A. Benamor, A. Amhamed, *ChemElectroChem* **2021**, *8*, 3207–3220.
[16] J. M. Spurgeon, B. Kumar, *Energy Environ. Sci.* **2018**, *11*, 1536–1551.
[17] M. Jouny, W. Luc, F. Jiao, *Ind. Eng. Chem. Res.* **2018**, *57*, 2165–2177.
[18] J. Hietala, A. Vuori, P. Johnsson, I. Pollari, W. Reutemann, H. Kieczka, *Ullmann's Encycl. Ind. Chem.* **2016**, 1–12.
[19] D. Higgins, C. Hahn, C. Xiang, T. F. Jaramillo, A. Z. Weber, *ACS Energy Lett.* **2019**, *4*, 317–324.
[20] K. Liu, W. A. Smith, T. Burdyny, *ACS Energy Lett.* **2019**, *4*, 639–643.
[21] E. W. Lees, B. A. W. Mowbray, F. G. L. Parlane, C. P. Berlinguette, *Nat. Rev. Mater.* **2022**, *7*, 55–64.
[22] J. B. Vennekoetter, R. Sengpiel, M. Wessling, *Chem. Eng. J.* **2019**, *364*, 89–101.
[23] R. Lin, J. Guo, X. Li, P. Patel, A. Seifitokaldani, *Catalysts* **2020**, *10*, 473.
[24] S. Litster, G. McLean, *J. Power Sources* **2004**, *130*, 61–76.
[25] F. Bidault, D. J. L. Brett, P. H. Middleton, N. P. Brandon, *J. Power Sources* **2009**, *187*, 39–48.
[26] U. O. Nwabara, E. R. Cofell, S. Verma, E. Negro, P. J. A. Kenis, *ChemSusChem* **2020**, *13*, 855–875.
[27] G. Díaz-Sainz, M. Alvarez-Guerra, J. Solla-Gullón, L. García-Cruz, V. Montiel, A. Irabien, *J. CO2 Util.* **2019**, *34*, 12–19.
[28] D. Kopljar, N. Wagner, E. Klemm, *Chem. Eng. Technol.* **2016**, *39*, 2042–2050.
[29] A. Del Castillo, M. Alvarez-Guerra, J. Solla-Gullón, A. Sáez, V. Montiel, A. Irabien, *J. CO2 Util.* **2017**, *18*, 222–228.
[30] B. De Mot, J. Hereijgers, M. Duarte, T. Breugelmans, *Chem. Eng. J.* **2019**, *378*, 122224.
[31] S. Sen, S. M. Brown, M. L. Leonard, F. R. Brushett, *J. Appl. Electrochem.* **2019**, *49*, 917–928.
[32] M. E. Leonard, M. J. Orella, N. Aiello, Y. Román-Leshkov, A. Forner-Cuenca, F. R. Brushett, *J. Electrochem. Soc.* **2020**, *167*, 124521.
[33] N. T. Nesbitt, T. Burdyny, H. Simonson, D. Salvatore, D. Bohra, R. Kas, W. A. Smith, *ACS Catal.* **2020**, *10*, 14093–14106.
[34] B. Kim, F. Hillman, M. Ariyoshi, S. Fujikawa, P. J. A. Kenis, *J. Power Sources* **2016**, *312*, 192–198.
[35] Y. Wu, S. Garg, M. Li, M. N. Idros, Z. Li, R. Lin, J. Chen, G. Wang, T. E. Rufford, *J. Power Sources* **2022**, *522*, 230998.
[36] L. M. Baumgartner, C. I. Koopman, A. Forner-Cuenca, D. A. Vermaas, *ACS Appl. Energy Mater.* **2022**, *5*, 15125–15135.
[37] A. A. Samu, I. Szenti, Á. Kukovecz, B. Endrődi, C. Janáky, *Commun. Chem.* **2023**, *6*, 41.
[38] H. Weinrich, B. Rutjens, S. Basak, B. Schmid, O. Camara, A. Kretzschmar, H. Kungl, H. Tempel, R.-A. Eichel, *MDPI Catal.* **2023**, submitted.
[39] N. Schmitt, M. Schmidt, G. Hübner, B. J. M. Etzold, *J. Power Sources* **2022**, *539*, 231530.
[40] L. M. Baumgartner, C. I. Koopman, A. Forner-Cuenca, D. A. Vermaas, *ACS Sustain. Chem. Eng.* **2022**, *10*, 4683–4693.
[41] M. J. Martínez-Rodriguez, C. Tong, S. Shimpalee, J. W. Van Zee, *ECS Meet. Abstr.* **2010**, *MA2010-02*, 927–927.
[42] U. O. Nwabara, A. D. Hernandez, D. A. Henckel, X. Chen, E. R. Cofell, M. P. De-Heer, S. Verma, A. A. Gewirth, P. J. A. Kenis, *ACS Appl. Energy Mater.* **2021**, *4*, 5175–5186.
[43] A. P. Young, J. Stumper, S. Knights, E. Gyenge, *J. Electrochem. Soc.* **2010**, *157*, B425.
[44] Y. Pan, H. Wang, N. P. Brandon, *J. Power Sources* **2021**, *513*, 1–77.
[45] A. Dutta, A. Kuzume, M. Rahaman, S. Vesztergom, P. Broekmann, *ACS Catal.* **2015**, *5*, 7498–7502.
[46] M. König, J. Vaes, E. Klemm, D. Pant, *iScience* **2019**, *19*, 135–160.
[47] P. Bumroongsakulsawat, G. H. Kelsall, *Electrochim. Acta* **2014**, *141*, 216–225.
[48] E. B. Easton, P. G. Pickup, *Electrochim. Acta* **2005**, *50*, 2469–2474.
[49] D. Zhang, G. Nagayama, *Langmuir* **2019**, *35*, 16508–16513.
[50] H. Yang, J. J. Kaczur, S. D. Sajjad, R. I. Masel, *J. CO2 Util.* **2020**, *42*, 101349.
[51] H. Yang, J. J. Kaczur, S. D. Sajjad, R. I. Masel, *J. CO2 Util.* **2017**, *20*, 208–217.
[52] Q. Wang, Y. Wu, C. Zhu, R. Xiong, Y. Deng, X. Wang, C. Wu, H. Yu, *Electrochim. Acta* **2021**, *369*, 137662.
[53] G. Wen, D. U. Lee, B. Ren, F. M. Hassan, G. Jiang, Z. P. Cano, J. Gostick, E. Croiset, Z. Bai, L. Yang, Z. Chen, *Adv. Energy Mater.* **2018**, *8*, 1–9.
[54] E. Irtem, T. Andreu, A. Parra, M. D. Hernández-Alonso, S. García-Rodríguez, J. M. Riesco-García, G. Penelas-Pérez, J. R. Morante, *J. Mater. Chem. A* **2016**, *4*, 13582–13588.
[55] R. Omrani, *PEM Fuel Cells* (Ed.: G. Kaur), Elsevier, Amsterdam, **2022**, pp. 91–122.
[56] A. El-Kharouf, T. J. Mason, D. J. L. Brett, B. G. Pollet, *J. Power Sources* **2012**, *218*, 393–404.
[57] G. Lin, T. Van Nguyen, *J. Electrochem. Soc.* **2005**, *152*, A1942.
[58] J. A. Abarca, G. Díaz-Sainz, I. Merino-Garcia, G. Beobide, J. Albo, A. Irabien, *J. Environ. Chem. Eng.* **2023**, *11*, 109724.
[59] H. Sadeghifar, *Energy Convers. Manag.* **2017**, *154*, 191–202.
[60] A. Del Castillo, M. Alvarez-guerra, J. Solla-gullón, A. Sáez, V. Montiel, A. Irabien, *Appl. Energy* **2015**, *157*, 165–173.
[61] I. Merino-Garcia, J. Albo, A. Irabien, *Nanotechnology* **2018**, *29*, 014001.
[62] "FlexCell User Manual," can be found under https://gaskatel.de/wp-content/uploads/Manual_TestCell_FlexCell_V2.pdf, **n.d**.

Manuscript received: March 16, 2023
Revised manuscript received: May 30, 2023
Version of record online: July 28, 2023